COMMISSIONING OF SUPERCONDUCTING-LINAC BOOSTER FOR RIKEN HEAVY-ION LINAC

N. Sakamoto*, M. Fujimaki, E. Ikezawa, H. Imao, O. Kamigaito, T. Nagatomo,
T. Nishi, K. Ozeki, K. Suda, A. Uchiyama, T. Watanabe, Y. Watanabe, K. Yamada
RIKEN Nishina Center, Wako, Japan

Abstract

The RIKEN heavy-ion linac was upgraded by the introduction of a new super-conducting linac-booster to further continue the super-heavy elements synthesis program beyond nihonium at the RIKEN Radioactive Isotope Beam Factory (RIBF) [1]. The total acceleration voltage was upgraded from 25 MV with 12 room temperature drift-tube-linacs (DTLs) to 39 MV. The superconducting linac (SRILAC) consists of 3 cryomodules based on 10 quarter wave resonators (QWRs) made from bulk niobium sheets and round rods. The superconducting QWR (SC-QWR) operated at 4.5 K, which was designed for acceleration of low-beta ions, operates at a frequency of 73.0 MHz in continuous wave (c.w.) mode. Two acceleration gaps provide an acceleration gradient (E_{acc}) of 6.8 MV/m for the ions with $\beta\,(\equiv v/c)$ of 0.078. After the commissioning of the cryomodules, an ^{40}Ar beam was successfully accelerated to 6.2 MeV/u for the first time. This paper provides an overview of the SC-Linac booster, its commissioning, and the first beam-acceleration test.

INTRODUCTION

In 2016, it was decided that the maximum beam current and total acceleration voltage of the RIKEN heavy-ion Linac (RILAC) would be upgraded to allow studies of super-heavy elements aimed at the synthesis of new super-heavy elements [2]. In this upgrade project, a new superconducting (SC) electron cyclotron resonance (ECR) ion source [3] and SC booster linac were developed and constructed. The original RILAC consists of six drift-tube-linac (DTL) tanks that are frequency-tunable from 17 to 45 MHz, and can accelerate heavy-ions to 2.9 MeV/u at 37.75 MHz. The new element nihonium (Nh) was synthesized by bombarding a ^{209}Bi target with an intense ^{70}Zn^{14+} beam with an energy of 5 MeV/u [4], accelerated by the RILAC, which was upgraded by the addition of a booster linac [5] consisting of six DTLs. The first two DTLs of the booster, A1 and A2, are equipped with short-plate frequency tuning systems to have a frequency range from 36 to 76 MHz, which will expand the energy range of the beam injected to the RIKEN Ring Cyclotron (RRC), while the latter four DTLs have a fixed frequency of 75.5 MHz. To preserve the versatility of the beams that are utilized for coupled operation of RILAC and RRC, it was decided to upgrade the RILAC by replacing the latter 4 DTLs of the booster linac, which are fixed-frequency cavities, with an SC-linac. The operational frequency of

73.0 MHz was selected after consideration of the future option to adapt the SC-linac to uranium acceleration at RIBF.

SUPERCONDUCTING LINAC BOOSTER

The design parameters of the SC-linac (SRILAC) are listed in Table 1 and its layout is shown in Fig. 1. The SRILAC consists of three cryomodules (CMs), CM1, CM2, and CM3, with room-temperature medium-energy beam transport (MEBT) between them. The design of the CMs is a modification of a prototype CM developed at RIKEN [6] as a part of the ImPACT Program [7]. The CMs contain neither SC magnets nor cold diagnostic devices. For the beam transport line connecting CMs, the so-called MEBT, a newly designed beam energy position monitor (BEPM) was employed instead of traditional wire scanners to avoid the generation of particulates that cause degradation of the cavity performance. It is also important to have an isolation system [8] between the existing room-temperature part where the vacuum pressure level is several $\times 10^{-5}$ Pa and the SRILAC to prevent contamination of the SC parts.

Table 1: Design Parameters of SRILAC

Parameters	
Frequency (MHz)	73.0 (c.w.)
E_{inj} (MeV/u)	3.6
E_{out} (MeV/u)	6.5
Maximum gap voltage (MV)	2.4
Synchronous phase (°)	-25
Number of cavities	10
Cavity type	QWR(TEM)
β_{opt}	0.078
TTF	0.9
R_{sh}/Q_0 (Ω)	579
G	22.4
E_{acc} (MV/m)	6.8
E_{peak}/E_{acc}	6.2
B_{peak}/E_{acc} (mT/(MV/m))	9.6
Operating temperature (K)	4.5
Target Q_0	1×10^9
Q_{ext}	$1 - 4.5 \times 10^6$
Amplifier output (kW)	7.5
Beam current (μA)	~ 100

The TEM cavities for the SRILAC are designed to operate in c.w. mode. The gap length of the cavity is optimized for β=0.078 particles with a transit time factor (TTF) of 0.9. The maximum gap voltage is 2.4 MV, which corresponds
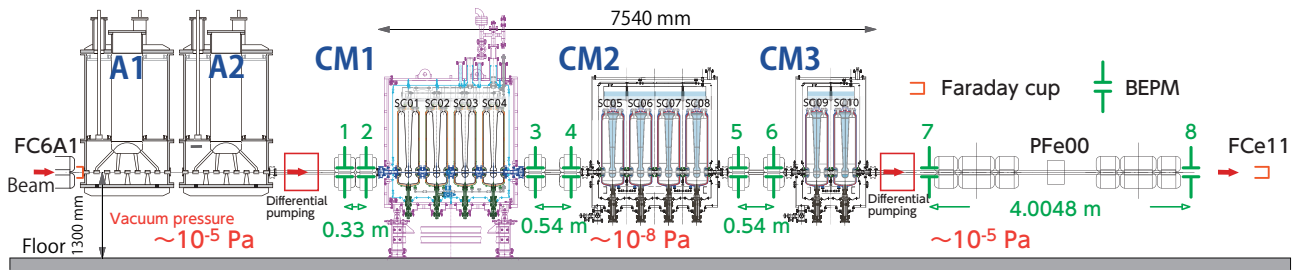
_____
* nsakamot@ribf.riken.jp

Figure 1: Layout of the SRILAC.

to an acceleration gradient E_{acc} of 6.8 MV/m with a synchronous phase of -25°. The cavities are made from pure Nb sheets with a residual resistivity ratio of 250, and their inner surfaces are processed by buffered chemical polishing (BCP1) with 100 μm, annealing at 750 °C for 3 h, light etching (20 μm, BCP2), and heat-treatment at 120 °C for 48 h. The operating temperature is 4.5 K and not 2 K, and all the cavities achieved fairly large Q_0 that exceeded the target value of 1×10^9 at an E_{acc} of 6.8 MV/m [9, 10]. Each bulk Nb cavity with a local magnetic shield of μ-metal is contained within a He vessel made of pure Ti.

The power coupler (PC) is designed with a tunable coupling so that a Q_{ext} range from 1×10^6 to 4.5×10^6 can be achieved by a change of the insertion distance of its antenna. The maximum beam current in the heavy-ion beams is 100 μA for the super-heavy element synthesis experiments; therefore, beam loading is negligible. A low Q_{ext} as small as 10^6 was selected to broaden the resonance curve with a $\pm$ 60 Hz operational-frequency-range achieved by an RF input power of 7.5 kW.

COMMISSIONING

Cryomodule and First Cool-down Test

Figure 2 shows a schematic of the CM1 and CM2 cryomodules. CM3, which contains two QWRs, is generally based on the same design as CM1 and CM2. The cold mass, which consists of cavities with a magnetic shield and a He vessel, a PC, and a dynamic tuner, is supported by thermal isolation pillars made of G10 from the bottom base plate; therefore, the CM is not a traditional top-loading type. Cavities are installed at an offset position to take thermal shrinkage into account. A design with a room-temperature single window was adopted for the PC instead of a double window coupler [11] to simplify the mechanical designs of the cryomodule and the coupler itself. The dynamic tuner coarsely changes the resonant frequency of the SC-QWRs to 73.0 MHz at 4.5 K and precisely compensates the frequency shift due to the He pressure deviation ($\Delta f / \Delta p = -2$ Hz/hPa) and the Lorentz detuning ($\Delta f = -35$ Hz @E_{acc} = 6.8 MV/m).

Each cavity is connected with beam bellows to separate the beam vacuum from the insulation vacuum of the cryomodule to prevent the ingress of particulates from dusty areas of the isolation vacuum. In addition to the local shielding
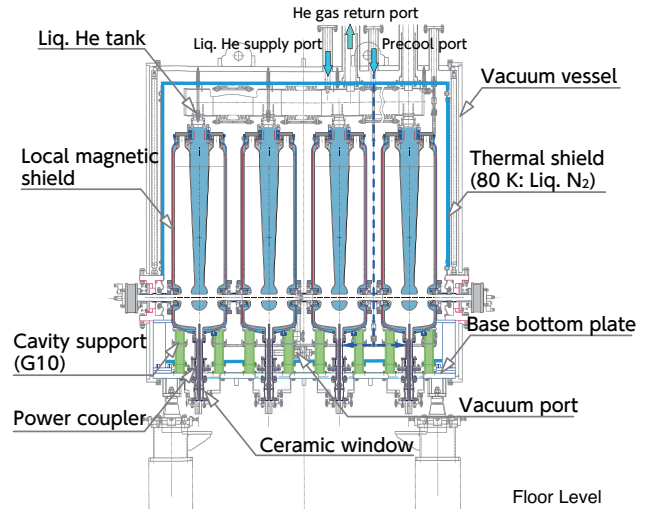

Figure 2: Schematic of SC-linac cryomodules.

placed inside the He vessel (see Fig. 2), the vacuum vessel is made of carbon steel rather than stainless steel to shield the external magnetic field efficiently. Thermal anchors connect the support pillars to the 80 K thermal shields, which are cooled by liquid nitrogen. The 80 K thermal shields also provide thermal anchors for the PCs and beam pipes.

The cold mass is cooled by 4.5 K liquid He provided by a liquid He cryogenic system using a HELIAL MF (Fig. 3) refrigerator (Air Liquide) combined with a MYCOM compressor. The cooling capacity of the cryogenic system was measured as 733 W at 4.5 K, while the electric power con-

Figure 3: Cold box and joint box are installed in the linac building.
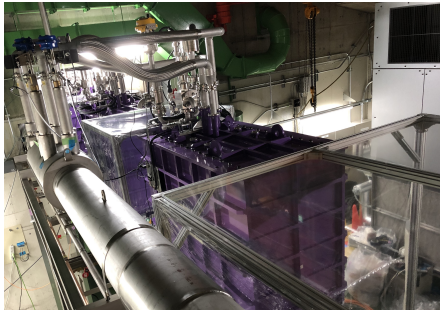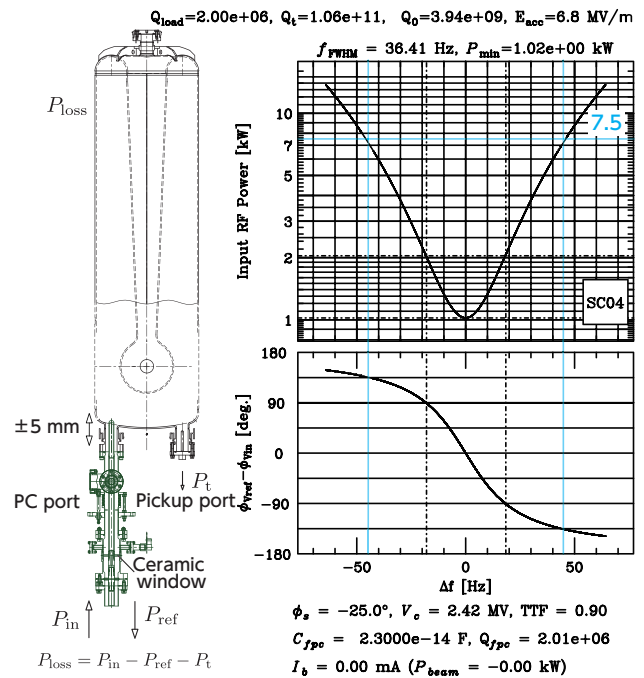
Figure 4: Liquid He transfer line and CMs.

Figure 5: External Q adjustment was performed by changing the PC insertion. The operational-frequency-range was calculated from an element circuit model as ± 45 Hz for $Q_{ext}(\approx Q_{loaded}) = 2 \times 10^6$.

sumption of the compressor is 300 kW. The operational He pressure of the He tank was set to 25 kPa and the maximum pressure was 37.5 kPa, which follows the high pressure safety regulation in Japan.

The CMs are connected with the He and N_2 transfer line with the U-tubes as shown in Fig. 4. The cool-down process was initiated on September 11, 2019 for the first time. First, He gas was flowed via a pre-cool line to the bottom part of cavities and the He gas gradually was cooled. During the first cool-down, a problem in the form of a vacuum leak of the isolation vacuum of the cold box occurred due to a defect in a T-pipe joint, which was quickly fixed by replacing the T-pipe joint. When the He temperature becomes 10 K, the main-supply valve is opened and then the pre-cool line valve is closed automatically so that cold He flows mainly via main-supply line. The liquid-He levels of the cryomodule He tanks finally reached the target levels and were stable on September 14, 2019. The liquid-He level of the He tank was well controlled by the supply-valve opening and the absolute pressure of the He was stabilized to be 125.9 ± 0.3kPa by controlling the return-valve. A typical warm-up process takes approximately 9 days to transfer He gas to a buffer tank (50 m^3).

Radio Frequency Test

Coupling adjustment of the PCs and resonant frequency measurement were performed at 4.5 K after cool-down. The coupler antenna insertion was set (see Fig. 5) so that the Q_{loaded} became approximately 1.5×10^6 using a network analyzer. Q_{loaded} of the SC04 cavity was 2×10^6 due to a malfunction of the sliding mechanism and its operational-frequency-range became ± 45 Hz, as shown in Fig. 5. After tuning of the $Q_{ext}(\approx Q_{loaded})$, all the cavities had resonant frequencies within the tuning frequency range between 0 and -14 kHz at 4.5 K. However, one of the SC-QWRs (SC05) had a vacuum leak from a coupler window. The coaxial power cable of SC05 was removed and a vacuum pump was connected to the PC port.

Subsequently, a high-power RF test was conducted. When the SC-QWRs were energized for the first time, multipacting phenomena at $E_{acc} < 0.1$ MV/m occurred. To overcome the low lying multipacting levels, the c.w. RF power was injected by adjusting the RF frequency to maximize the conditioning effect by observation of the pickup signal level

and the vacuum pressure. On average, it took 3 to 4 h for each cavity. No additional conditioning has been required to date. A self-excited loop mode is utilized by energizing from zero gap-voltage. Note that the multipacting levels of 0.4 MV/m and 0.8 MV/m observed in the bulk-cavity RF test [9] were easily overcome due to the strong coupling of the PC.

Mitigation of the effect on the RF-field stability of the cavity microphonics is one of the major issues for SC linacs. The SC-QWR for SRILAC has a rigid structure against pendulum oscillation modes with its conical stem and mechanical ribs on the top part. Substantial modulation was observed for an RF-field pickup signal at around 50 Hz [12]. The RF resonant frequency of the SC-cavity fluctuates according to the degree of mechanical vibration. This causes fluctuation of the resonant curve and then modulation of the RF-field, i.e., the phase-amplitude modulation, which is expected to be mitigated using a feedback system of a low level RF (LLRF).

Figure 6A shows a block diagram of the RF system for SRILAC. The maximum output power of the RF amplifier is 7.5 kW. The amplifier, of which the output impedance is $50 \, \Omega$, is capable of c.w. operation with open and short terminations in the absence of an external circulator. According to the phase difference between the forward and reflected signal from a directional coupler inserted to the RF-power transmission line, the dynamic tuner is driven automatically to maintain the resonant frequency around 73 MHz.

The feedback system (LLRF) is based on a high-performance programmable logic chip (FPGA-Xilinx
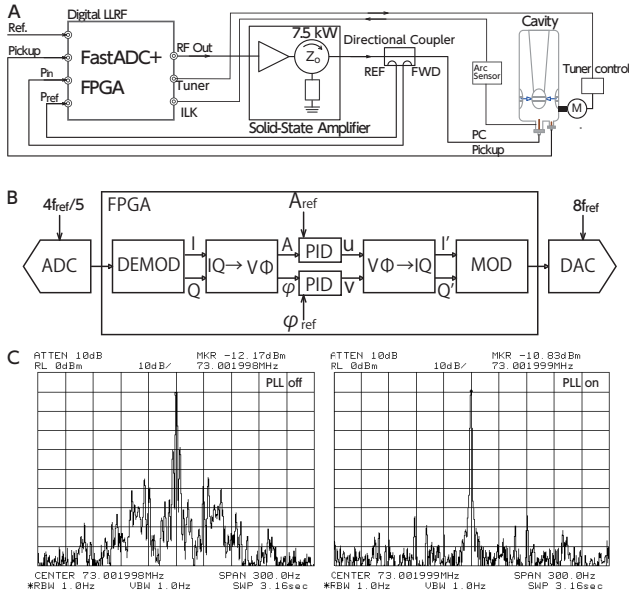
Figure 6: (A) RF block diagram, (B) block diagram of LLRF, and (C) comparison between pickup signal spectra with phase lock off (left) and on (right).

Figure 7: Phase scan plot, where E_{out} is plotted as a function of the RF-field phase for each cavity.

XC6SLX150-2FGG484C; Fig. 6B). The RF-field pickup signal and the signals from the directional couplers are digitized by harmonic sampling in sync with the 4/5 frequency of the reference signal (73.0 MHz). Converted digital signals are first demodulated to I-Q components, and then converted to amplitude-phase components.

Figure 6C shows the cavity pickup signal spectra with phase lock on and off as an example. The side-band components due to microphonics around ± 50 Hz apparent in Fig. 6C(left) are successfully removed by turning on the phase lock loop (PLL), as shown in Fig. 6C(right).

First Beam-acceleration Test

According to the requirement for super-heavy element synthesis experiments, an ^{40}Ar beam was accelerated for the first beam-acceleration test. However, one of the SC-QWRs (SC05) was not available; therefore, the acceleration energy was lowered to 6.2 MeV/u from 6.5 MeV/u.

The ^{40}Ar^{13+} beam with an intensity of approximately 23 enA (duty 3%, chopper frequency 1 kHz) was accelerated to 6.2 MeV/u with a gap voltage of 1.13 MV. For the SC-linac tuning, SC-QWRs were energized one by one and the beam energy was measured with systematic variation of the RF-field phase (see Fig. 7). The beam energy was precisely obtained for step by step time-of-flight (TOF) measurement with a pair of BEPMs [13, 14], as indicated in Fig. 1, with a low beam current. The synchronous phase $\phi_s = -25°$ was obtained by shifting the RF-field phase from the zero acceleration/bunching phase by 65 deg. towards the top of the sine curve. The beam position remained almost at the center of beam aperture during the phase scan due to geometrical correction by the steering effect of the QWR cavity [9]. The accelerated beam energy successfully
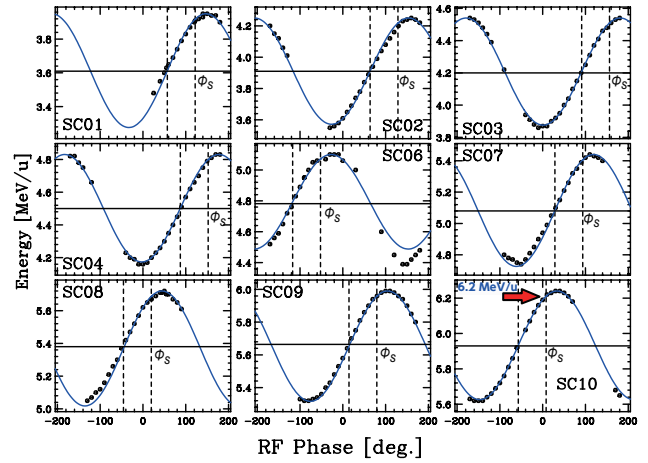
reached 6.2 MeV/u at 9PM on January 28th, 2020. The absolute value of the gap voltage was corrected by the measured beam energy as listed in Table 2.

Table 2: Cavity Voltage Correction by Measurement of the Beam Energy

Cavity	E_{out} MeV/u	Gap voltage Calc.	Gap voltage Actual	Correction factor
A2	3.613	-	-	
SC01	3.911	1130	1064.1	1.062
SC02	4.208	1130	1090.2	1.037
SC03	4.502	1130	1130.9	0.999
SC04	4.794	1130	1142.7	0.989
SC05	5.083	-	-	-
SC06	5.083	1130	1048.9	1.077
SC07	5.369	1130	1058.8	1.067
SC08	5.653	1130	1103.3	1.024
SC09	3.933	1130	1051.0	1.075
SC10	6.211	1130	1130.6	0.999

After an elaborate tuning, the transmission efficiency from FC6A1 to FCe11 in Fig. 1 reached 100% with a beam current of 6.11 eμA. The vertical and horizontal beam position monitored by BEPM was centralized and the beam loss which occurred at the MEBT was minimized keeping the deterioration of the vacuum pressure below 1×10^{-7} Pa. The beam emittance measurement by Q-scan is reported in Ref. [15].

The field emission level measurement was performed after the first beam-acceleration test. While no emission was observed in the vertical test [9], field emission was observed for each cavity (Fig. 8). No significant cryogenic consumption has occurred to date. The emission level is routinely measured every time after cool-down.
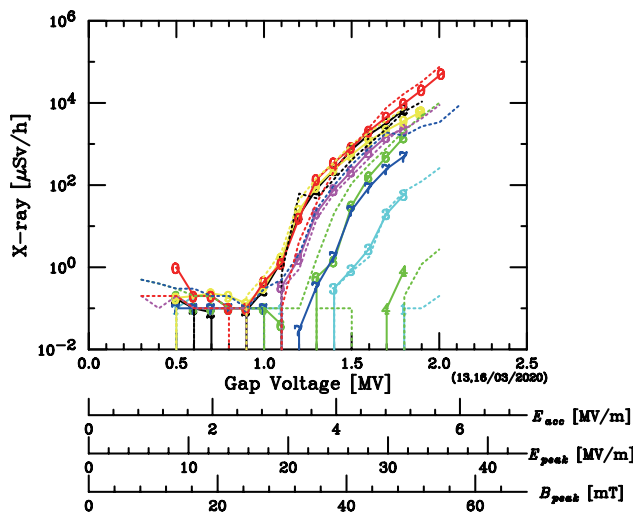
Figure 8: X-ray emission as a function of E_{acc} for each cavity. The solid and dashed lines are the emission level measured on March 13-16, 2020 before the 3rd beam-acceleration test that measured on February 19, 2020 before the 2nd beam-acceleration test, respectively. The emission level rise indicates deterioration of performance of the SC-cavities.

SUMMARY AND OUTLOOK

An upgrade of RIKEN heavy-ion linac was conducted by the introduction of a new SC linac-booster that consists of 3 cryomodules based on 10 TEM QWRs made from bulk niobium for c.w. heavy-ion beams. A cool-down test and RF test with an operational temperature of 4.5 K were performed without significant trouble, except SC05 encountered a vacuum leakage from the ceramic window of the coupler. Q_{ext} for each cavity was tuned to be 1.5×10^6 after cool-down. A new solid-state amplifier and digital LLRF provide a stable RF-field. The ^{40}Ar beam was successfully accelerated to 6.2 MeV/u with an intensity of 0.47 pμA in the first beam acceleration test.

A ^{51}V^{13+} beam with an energy from 4.2 MeV/u to 6.3 MeV/u was delivered for a user service time. To achieve a beam current of 10 pμA, analysis of the transmission efficiency of the low-energy part of the RILAC and optimization of the beam transport of the SRILAC are currently underway. The data archive system [16] for the many accelerator parameters, including not only RF-field of the rf cavities, but also excitation current of the magnets, vacuum, temperature of the cooling water, and BEPMs, is very helpful to understand what occurs during beam tuning. Newly developed digital LLRF is planned to be adopted to each RF system of the RT-DTLs, RFQ, and bunchers to improve the stability of their RF-field.

User service will start in October of this year (2020) after the annual maintenance is completed.

ACKNOWLEDGEMENT

REFERENCES

[1] H. Okuno, N. Fukunishi, and O. Kamigaito, Prog. Theor. Exp. Phys. 03C002(2012).

[2] O. Kamigaito *et al.*, "Present Status and Future Plan of RIKEN RI Beam Factory", in Proc. IPAC'16, Busan, Korea, May 2016, paper TUPMR022, p. 1281.

[3] T. Nagatomo *et al.*, Rev. Sci. Instrum. **91**,023318(2020).

[4] O. Kamigaito, "RIBF Accelerators and Synthesis of the New Element [113]", Proc. 13th PASJ Annual Meeting, Chiba, Japan, Sep. 2020, paper MOOLP03, p. 9.

[5] O. Kamigaito *et al.*, Rev. Sci. Instrum. **76**,013306(2005).

[6] N. Sakamoto *et al.*, "Development of Superconducting Quarter-Wave Resonator and Cryomodule for Low-Beta Ion Accelerators at RIKEN Radioactive Isotope Beam Factory", Proc. SRF2019, Dresden, Germany, paper WETEB1, p. 750-757.

[7] http://www.jst.go.jp/impact/en/program/08.html

[8] H. Imao *et al.*, "Non-Evaporative Getter-Based Differential Pumping System for SRILAC at RIBF", Proc. SRF2019, Dresden, Germany, paper TUP013, p. 419-423.

[9] N. Sakamoto *et al.*, "Construction Status of the Superconducting Linac at RIKEN RIBF", Proc. LINAC2018, Beijing, China, paper WE2A03, p. 620-625.

[10] K. Yamada *et al.*, "Construction of Superconducting Linac Booster for Heavy-Ion Linac at RIKEN Nishina Center", Proc. SRF2019, Dresden, Germany, TUP037, p. 504-509.

[11] K. Ozeki *et al.*, "Design of Input Coupler for RIKEN Superconducting Quarter-Wavelength Resonator",Proc. SRF2015, Whistler, BC, Canada, paper THPB084, p. 1335-1339.

[12] O. Kamigaito *et al.*, "Measurement of Mechanical Vibration of SRILAC Cavities", Proc. SRF2019, Dresden, Germany, TUP042, p. 513-517.

[13] T. Watanabe *et al.*, "Calibration for Beam Energy Position Monitor System for Riken Superconducting Acceleration Cavity", Proc. IBIC2019, Malmö, Sweden, paper WEPP007, p. 526-529.

[14] T. Watanabe *et al.*, "Commissioning of the Beam energy position monitor system for the Superconducting RIKEN Heavy-ion Linac", Proc. 17th PASJ Annual Meeting, Sep. 2020, paper FRPP22, this meeting.

[15] T. Nishi *et al.*, "Emittance measurement and ion optics tuning for SRILAC beamline", Proc. 17th PASJ Annual Meeting, Sep. 2020, paper THOO08, this meeting.

[16] A. Uchiyama *et al.*, "Introduction of Archiver Appliance to RILAC control system", Proc. 17th PASJ Annual Meeting, Sep. 2020, paper FRPP26, this meeting.